Influence of rarefaction on the flow dynamics of a stationary supersonic hot-gas expansion

G. Abbate* and C. R. Kleijn
Department of Multi-Scale Physics and J.M. Burgers Centre for Fluid Mechanics, Delft University of Technology, Prins Bernhardlaan 6, 2628 BW Delft, The Netherlands

B. J. Thijsse
Department of Materials Science and Engineering, Delft University of Technology, Mekelweg 2, 2628 CD Delft, The Netherlands

R. Engeln, M. C. M. van de Sanden, and D. C. Schram
Department of Applied Physics, Eindhoven University of Technology, P.O. Box 513, 5600 MB Eindhoven, The Netherlands
(Received 30 November 2007; published 12 March 2008)

The gas dynamics of a stationary hot-gas jet supersonically expanding into a low pressure environment is studied through numerical simulations. A hybrid coupled continuum-molecular approach is used to model the flow field. Due to the low pressure and high thermodynamic gradients, continuum mechanics results are doubtful, while, because of its excessive time expenses, a full molecular method is not feasible. The results of the hybrid coupled continuum-molecular approach proposed have been successfully validated against experimental data by R. Engeln *et al.* [Plasma Sources Sci. Technol. **10**, 595 (2001)] obtained by means of laser induced fluorescence. Two main questions are addressed: the necessity of applying a molecular approach where rarefaction effects are present in order to correctly model the flow and the demonstration of an invasion of the supersonic part of the flow by background particles. A comparison between the hybrid method and full continuum simulations demonstrates the inadequacy of the latter, due to the influence of rarefaction effects on both velocity and temperature fields. An analysis of the particle velocity distribution in the expansion-shock region shows clear departure from thermodynamic equilibrium and confirms the invasion of the supersonic part of the flow by background particles. A study made through particles and collisions tracking in the supersonic region further proves the presence of background particles in this region and explains how they cause thermodynamic nonequilibrium by colliding and interacting with the local particles.

DOI: 10.1103/PhysRevE.77.036703 PACS number(s): 47.11.−j, 47.40.Ki, 47.45.−n, 52.65.Ww

I. INTRODUCTION

Several gas fluidic applications of current technological importance involve a gas jet supersonically expanding into vacuum or into a low pressure environment. Examples include gas thruster nozzles and plume flows [1] and processes of thin film deposition, etching, and passivation from expanding plasma or gas jets [2].

An interesting issue connected to this kind of flow is the transition from continuum to rarefied regime. The gas in the jet is generally at relatively high pressure, and then it rapidly expands into a low pressure environment. For this reason, the gas first supersonically expands and then quickly compresses through a stationary shock wave (the so-called Mach disk). In addition, the expansion zone is surrounded by a barrel shaped shock (the so-called barrel shock). Because of the low environment pressure and high thermodynamic gradients in the shock region, the flow undergoes a spatial transition from the low Knudsen number (Kn) continuum regime to the high Knudsen number rarefied regime.

Although several studies have been devoted to supersonic expansion of gas jets in vacuum or low pressure environment [3–20], full understanding of the processes governing the flow has not been reached yet. In particular, it is still not completely clear how important the influence of the rarefaction effects is on the dynamics of the flow [17]. Another important question is whether the barrel shock, which becomes transparent to background molecules due to rarefaction effects, still protects the supersonic part of the flow [8]. We call background molecules the molecules that are present outside the expansion-shock region. These background molecules could, therefore, invade the supersonic part of the jet, influencing its properties. Already Fenn and Anderson in 1966 [3] and Campargue in 1970 [4] predicted this phenomenon, but a full understanding of it has not yet been given.

In the current paper these last two issues will be addressed: (i) the importance of rarefaction effects on the flow field and (ii) the study of the presence of background particles in the supersonic region. These issues will be studied through detailed numerical simulations of the flow, pressure, and temperature distributions in the expanding jet and its surroundings.

It has been shown [17] that, because of rarefaction effects, the continuum computational fluid dynamics (CFD) approach fails in predicting temperature and velocity fields in the shock region. These can be correctly studied only with the help of kinetic simulations accounting for rarefaction and nonequilibrium effects. For this reason, in the past, direct simulation Monte Carlo (DSMC) has been used [17], but with a too coarse mesh in the near-inlet region. However, because DSMC computational expenses scale with Kn^{-4}, it is practically impossible to fulfill the DSMC requirements (e.g., the mesh size should be smaller than one-third of the

*G.Abbate@tudelft.nl

mean free path), especially near the inlet, where the Knudsen number is quite low [17].

In order to overcome this problem and to accurately simulate the above types of gas flows, one needs to construct a model that on the one hand accounts for the molecular nature of the gas flow where needed, and on the other hand uses a continuum model where allowed. In recent years several hybrid continuum-molecular models have been proposed [21–27].

In particular, in this paper we use a hybrid coupled continuum-DSMC approach [27] to model the problem; we apply the continuum CFD approach in the wide continuum region in order to save computational time, and DSMC only in the expansion-shock region where it is necessary in order to correctly model the rarefied nature of the flow.

In Sec. II we first describe the studied configuration and experiments used to validate our simulations. The explanation of the hybrid numerical simulation method is given in Sec. III. The results of our simulations of a stationary supersonic hot gas expansion are presented in Sec. IV and compared against (published) experimental data. In particular, in this section we focus on the rarefaction effects, and we show a numerical demonstration of the invasion of the supersonic region by the background molecules.

II. STUDIED CONFIGURATION AND MEASUREMENT TECHNIQUE

In order to have an experimental support to our conclusions, all our numerical results will be validated by comparing them to experimental measurement by Engeln *et al.* [8]. The measurements described in [8] were performed on an expanding thermal plasma jet. Nevertheless, because of the low ionization degree, they can be used to validate our present results on a neutral gas flow, composed only of argon atoms, neglecting the presence of electrons and ions [8] and the effects of ionization and recombination on the flow field. It has been shown, in fact, that ionization is practically absent in this flow [8], and even if the recombination can be significant, it affects only the electron temperature field and not the gas temperature and velocity fields [28].

The experimental setup in which the expanding thermal plasma jet is created has been extensively described elsewhere [29]. The transport of neutral argon atoms is studied by means of laser induced fluorescence spectroscopy (LIF). A detailed description of the LIF technique is given elsewhere [8]. The velocity w along the laser beam of groups of atoms is measured. From the first moment of the velocity distribution the average velocity is determined, while the second moment is related to the temperature.

Although the LIF measurements are performed on argon atoms in the metastable and resonant states, it is argued in [8] that the velocity distribution of these atoms reflects the velocity distribution of the ground state atoms.

III. NUMERICAL SIMULATION METHOD

In order to properly characterize the various regimes in the gas flow, the Knudsen number Kn is defined as the ratio between the mean free path and a relevant macroscopic length scale. When Knudsen is small ($\mathrm{Kn}<0.01$), the gas may be treated as a continuum and the gas flow may be modeled using CFD (computational fluid dynamics). When Knudsen is large ($\mathrm{Kn}>10$), the gas behavior is entirely molecular and may be modeled using molecular dynamics techniques. In the intermediate regime, the DSMC (direct simulation Monte Carlo) approach is the most commonly used simulation technique. However, its computational expenses scale with Kn^{-4}, and become inadmissible for Kn smaller than ~ 0.05.

In order to overcome this dilemma and accurately solve the flow throughout the expanding gas jet, we use a hybrid CFD-DSMC model, which takes into account the molecular nature of the gas flow where needed, and uses a continuum model where allowed.

A. Continuum algorithm: CFD

The CFD code used for solving the Navier-Stokes equations in the low Kn number regions is an unsteady solver based on a finite volume formulation in compressible form. It uses an explicit first-order time integration in combination with a second-order spatially accurate, flux-splitting, MUSCL scheme Riemann solver for the Navier-Stokes equations [30,31]. An explicit scheme, although computationally more expensive, is used because it is more accurate and because computational expenses of the CFD solver are small compared to those of the DSMC solver anyhow. Temperature dependent viscosities and thermal conductivities are computed from kinetic theory [32]. The pressure is computed from the ideal gas law.

B. Molecular algorithm: DSMC

Direct simulation Monte Carlo is a well-established algorithm for computing rarefied gas dynamics at the level of the Boltzmann equation; the algorithm is described in more detail in [33].

In order to accurately model viscous effects, the variable soft spheres (VSS) model is used to calculate particle cross sections. For the implementation of inlet or outlet boundary conditions, a "buffer zone" or "particle reservoir" approach is used [34]. A Chapman-Enskog [35] distribution is used to create particles in those reservoirs. The Chapman-Enskog distribution is obtained as an approximate solution of the Boltzmann equation and is expressed as a product of a local Maxwellian and a polynomial function of the thermal velocity components. It has been demonstrated that in a hybrid continuum-DSMC method a Chapman-Enskog distribution, rather than a simple Maxwellian distribution, is required when the viscous fluxes are taken into account [36,37].

C. Determination of the continuum-DSMC interface

An important issue in developing a coupled continuum-DSMC method is how to determine the appropriate computational domains for the DSMC and continuum solvers, and the proper interface boundary between these two domains. The continuum breakdown parameter $\mathrm{Kn}_{\max}$ [38] is em-

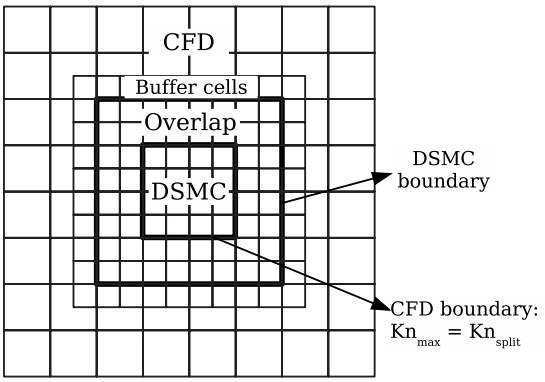

FIG. 1. Illustration of the Schwarz coupling method in a 2D geometry.

ployed in the present study as a criterion for selecting the proper solver

$$\mathrm{Kn}_{\max} = \max[\mathrm{Kn}_{\rho}, \mathrm{Kn}_{V}, \mathrm{Kn}_{T}] \tag{1}$$

where Kn_{ρ}, Kn_{V}, and Kn_{T} are the local Knudsen numbers based on density, velocity, and temperature length scales, according to

$$\mathrm{Kn}_{Q} = \frac{\lambda}{Q_{\mathrm{ref}}} |\nabla Q|. \tag{2}$$

Here, Q is a flow property (density ρ, velocity V, or temperature T) and λ is the local mean free path length. Q_{ref} is a reference value for Q, which can either be its local value, or a typical value. If the calculated value of the continuum breakdown parameter in a region is larger than a limiting value $\mathrm{Kn}_{\mathrm{split}}$, then that region cannot be accurately modeled using the continuum approach, and DSMC has to be used.

D. Schwarz coupling

The proposed coupling method for steady flows has been described in detail in [27]. It is based on the Schwarz method [25] and it consists of two stages. The first stage is a prediction stage, where the unsteady Navier-Stokes (NS) equations are integrated in time using CFD on the entire domain Ω until a steady state is reached. From this steady state solution, the continuum breakdown parameter $\mathrm{Kn}_{\max}$ is computed everywhere in Ω and its values are used to split Ω in the subdomains Ω_{DSMC} ($\mathrm{Kn}_{\max} > \mathrm{Kn}_{\mathrm{split}}$), where the flow field will be evaluated using DSMC, and Ω_{CFD} ($\mathrm{Kn}_{\max} < \mathrm{Kn}_{\mathrm{split}}$), where the continuum solver will be used. For $\mathrm{Kn}_{\mathrm{split}}$ a value of 0.05 was used. Between the DSMC and CFD regions an overlap region is considered, where the flow is computed with both the DSMC and the CFD solver (Fig. 1). This overlap region is chosen to be located entirely in the $\mathrm{Kn}_{\max} > \mathrm{Kn}_{\mathrm{split}}$ region.

In the second stage, DSMC and CFD are run in their respective subdomains with their own time steps (Δt_{DSMC} and Δt_{CFD}, respectively), until a steady state is reached. First, DSMC is applied; molecules are allocated in the DSMC subdomain according to the density, velocity, and temperature obtained from the initial CFD solution. A Chapmann-Enskog distribution is chosen to create molecules. The grid is automatically refined in the DSMC region in order to respect the DSMC requirements (i.e., the size of grid cells in the DSMC zone should not exceed $\frac{\lambda}{3}$). The boundary conditions to the DSMC region come from the solution in the CFD region. As described in the previous section "particle reservoir cells" are considered outside the overlapping region. In these cells molecules are created according to the density, velocity, and temperature and their gradients in the CFD solution with a Chapmann-Enskog distribution.

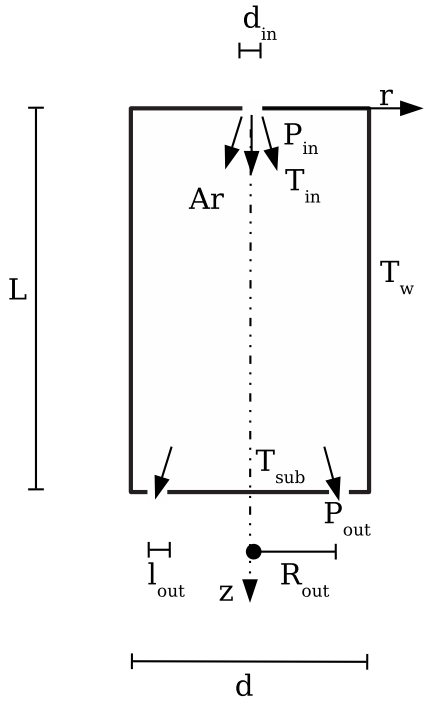

FIG. 2. Scheme of the low pressure chamber. (Diagram not to scale.)

After running the DSMC, the NS equations are solved in the CFD region. The boundary conditions come from the solution in the DSMC region, averaged over the CFD cells.

Once a steady state solution has been obtained in both the DSMC and NS regions, the continuum breakdown parameter $\mathrm{Kn}_{\max}$ is reevaluated and a new boundary between the two regions is computed. This second stage is iterated until in the overlapping region the relative difference (in pressure, velocity, and temperature) between the DSMC and CFD solutions is less than a prescribed small value.

E. Modeled geometry

The computational domain (Fig. 2) is a $d=32$ cm diameter cylinder of length $L=50$ cm. From a circular hole of diameter $d_{\mathrm{in}}=8$ mm, on its top, a flow of 56 sccs of argon is injected at a temperature $T_{\mathrm{in}}=8000$ K. The top and lateral walls are at a temperature $T_w=400$ K, while the bottom wall, which represents the substrate, is at a temperature $T_{\mathrm{sub}}=600$ K.

The pumping exit, which in reality is a circular hole, in our 2D model has been represented as a $l_{\mathrm{out}}=2$ cm wide ring on the bottom of the cylinder at a distance of $R_{\mathrm{out}}=12$ cm

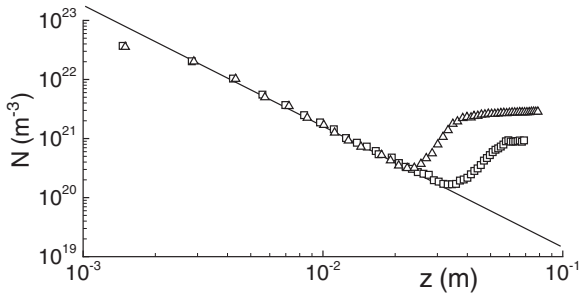

FIG. 3. Number density distribution along the z axis in the expansion-shock region evaluated by the hybrid approach at 20 Pa (□) and 100 Pa (△) chamber pressures.

from the axis. Two different pressures P_{out} in the exit have been considered, respectively, 20 and 100 Pa.

Inside the chamber we suppose the flow to be 2D axisymmetric. The continuum grid is composed of 100 cells in the radial direction and 200 cells in the axial direction. The cells are slightly stretched in the radial direction with a ratio of 1.65 between the size of the last and the first cell. The code automatically refines the mesh in the DSMC region to fulfill its requirements.

IV. RESULTS AND DISCUSSION

A. Rarefaction effects

In the following Fig. 3 the number density profiles along the z axis in the expansion-shock region evaluated by the hybrid approach for the two considered chamber pressure conditions (respectively, 20 and 100 Pa) are shown. The calculated densities show the typical $1/z^2$ dependence in the expansion.

In order to describe the effects of rarefaction on the flow field, it is important to identify the region where these effects take place. For this reason, in Figs. 4 and 5 we show the continuum breakdown parameter Kn_{max} in the chamber and the consequent division between the DSMC, continuum, and overlapping regions in our hybrid method, respectively, for 20 and 100 Pa chamber pressures.

In both 20 and 100 Pa chamber pressure cases, there are various counteracting effects influencing the value of Kn_{max}: as a result of the decrease in pressure, the mean free path increases from the inlet to the exit of the chamber. As a result of the cooling of the gas, the temperature decreases from the inlet to the exit of the chamber and the opposite effect occurs. And finally, smaller local gradient length scales are present near the inlet and in the shock, than in the rest of the chamber. The overall effect is that the continuum breakdown parameter is small near the inlet, then it increases becoming high in the expansion-shock region, and finally, it becomes low again in the rest of the chamber. Also near the substrate wall the continuum breakdown parameter increases, due to steep velocity and temperature gradients, but not to values exceeding Kn_{split}. This means that the flow first undergoes a continuum-rarefied transition in the near-inlet region, and then a rarefied-continuum transition downstream of the shock [Figs. 4(b) and 5(b)]. By comparing Fig. 4(a) to Fig. 5(a), it is also clear that, as expected, the overall values of the continuum breakdown parameter decrease if we increase the pressure in the chamber. As a consequence of that, going from 20 Pa to 100 Pa, the size of the region where the use of DSMC is necessary to correctly model the flow is reduced [Figs. 4(d) and 5(d)].

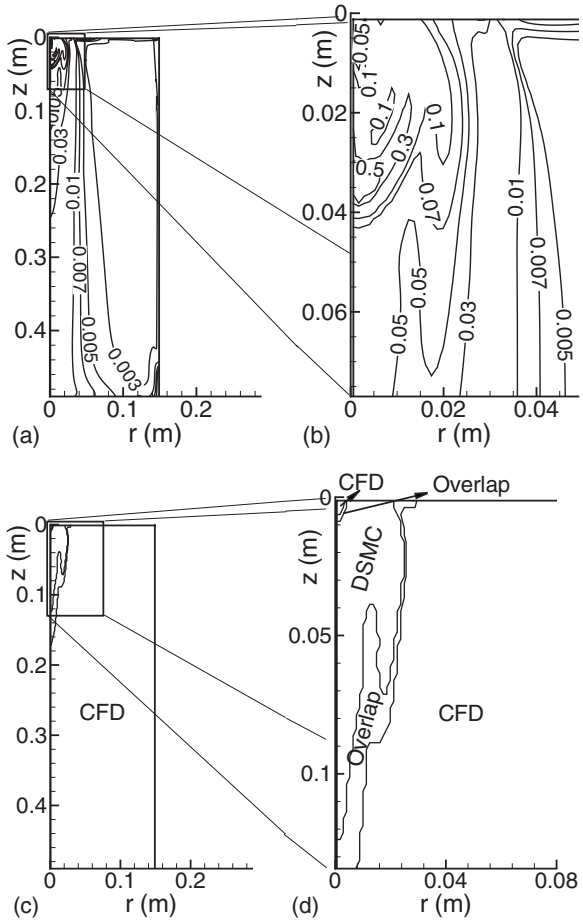

FIG. 4. Contours of the continuum breakdown parameter Kn_{max} in the entire chamber (a), and zoomed in to the expansion-shock region (b), CFD/DSMC domains splitting in the entire chamber (c), and zoomed in to the expansion-shock region (d), for 20 Pa chamber pressure.

Temperature and velocity fields obtained with the coupled CFD/DSMC at 20 and 100 Pa chamber pressures are compared to results from a full continuum CFD simulation in Figs. 6 and 7, respectively. It should be noted that DSMC simulations intrinsically contain statistical scatter, explaining why the contours in the hybrid simulations are less smooth than in the continuum simulations. From an analysis of the figures, it is evident that far away from the expansion-shock region, the two methods give very similar results [Figs. 6(a) and 6(c) and Figs. 7(a) and 7(c)]. The use of DSMC in the hybrid method influences only the region where rarefaction effects are present. Far away from the expansion-shock region, the influence of rarefaction effects is negligible. As expected, the two approaches differ more at 20 Pa chamber pressure than at 100 Pa, since stronger rarefaction effects are present at 20 Pa than at 100 Pa.

At 20 Pa the hybrid method predicts a stronger expansion compared to the continuum method, reaching a lower tem-

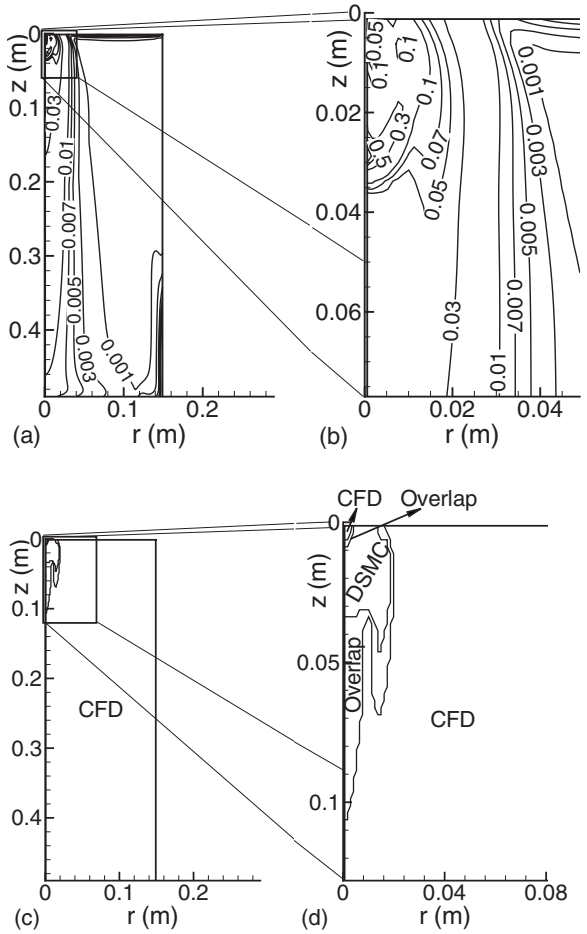

FIG. 5. Contours of the continuum breakdown parameter Kn_{max} in the entire chamber (a), and zoomed in to the expansion-shock region (b), CFD/DSMC domains splitting in the entire chamber (c), and zoomed in to the expansion-shock region (d), for 100 Pa chamber pressure.

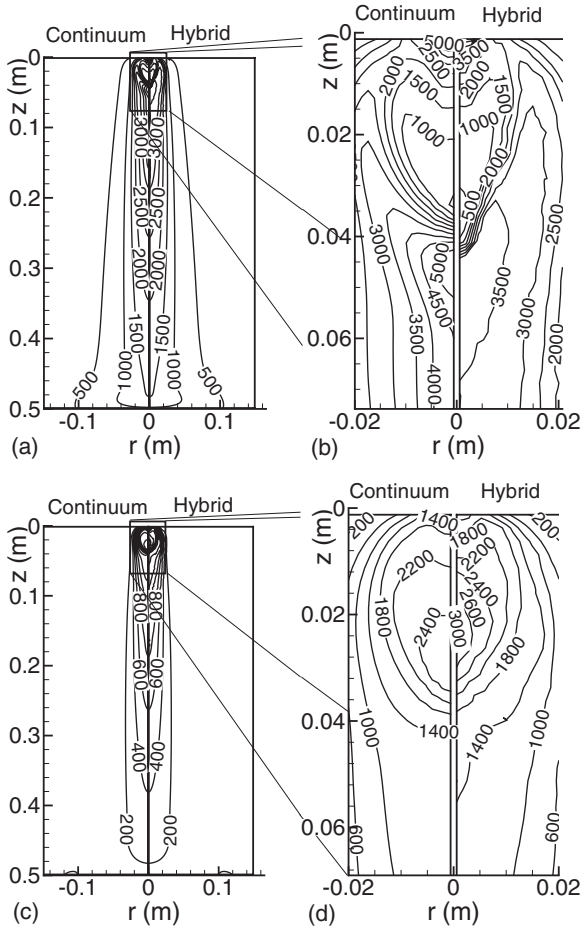

FIG. 6. Temperature field (in K) in the entire chamber (a), and zoomed in to the expansion-shock region (b) and velocity field (in m/s) in the entire chamber (c), and zoomed in to the expansion-shock region (d), for 20 Pa chamber pressure.

perature [Fig. 6(b)] and higher velocity [Fig. 6(d)]. Also, compared to the full continuum simulation, the shock is slightly moved downstream along the z axis in the hybrid simulation. Finally, after the shock the temperature predicted by the hybrid method is significantly (500–1500 K) lower than the one calculated by the continuum approach.

At 100 Pa only small differences between the two methods are present in the temperature fields [Fig. 7(b)]. The differences in the velocity fields, on the contrary, are more significant [Fig. 7(d)]; in the expansion, in fact, the hybrid method reaches higher values of the velocity than the continuum approach. The position of the shock is the same and both methods describe a further small expansion and shock after the first stronger ones.

In order to further clarify the effects of rarefaction on the flow field, Figs. 8 and 9 show, respectively for the temperature and the velocity along the z axis, a comparison between the present hybrid method, the present continuum simulation, results from full DSMC simulations performed by Selezneva *et al.* [17], and experimental data from [8] at both 20 Pa (a) and 100 Pa (b) chamber pressures. Although there is quite some scattering in the experimental data, in all cases it is clear that the hybrid method predicts the experimental data better than the other approaches. It is important to explain that the reason why the hybrid approach predicts experimental data even better than the full DSMC simulations, in the current case, is that, as discussed in Sec. I and as already highlighted by Selezneva *et al.* [17], in the full DSMC simulations it was not possible to respect DSMC requirements in the near-inlet region and a too coarse mesh had to be used.

If we first compare the results of the hybrid CFD/DSMC approach to those of the full CFD approach, Fig. 8(b) shows that even at 100 Pa chamber pressure, the hybrid approach follows much better than the continuum approach the experimental data in the shock and aftershock region. As we reduce the chamber pressure [Fig. 8(a)], we further increase the rarefaction effects. In the continuum approach the shock wave appears too early and the temperature after the shock is too high, whereas in the hybrid approach the shock moves forward due to rarefaction and the temperature after the shock is lower.

Figure 9 demonstrates that the continuum approach is unable to quantitatively predict the velocity profile and maximum velocity in the expansion-shock region at neither 20 Pa (a) nor 100 Pa (b) chamber pressures, and is quantitatively correct only downstream of the expansion-shock region as already shown in [17]. Because of rarefaction, upstream of

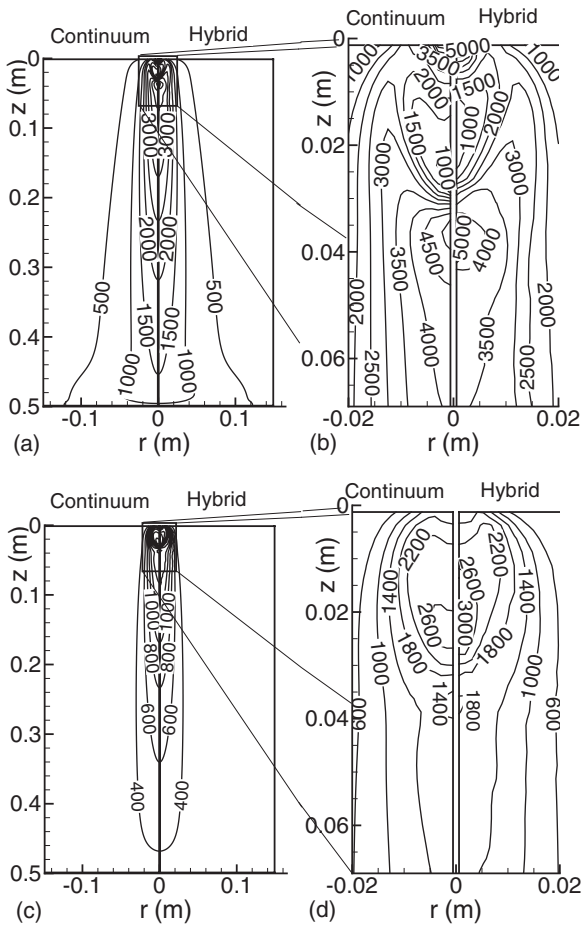

FIG. 7. Temperature field (in K) in the entire chamber (a), and zoomed in to the expansion-shock region (b) and velocity field (in m/s) in the entire chamber (c), and zoomed in to the expansion-shock region (d), for 100 Pa chamber pressure.

the shock the expansion is stronger, reaching higher velocity values at both 20 and 100 Pa chamber pressure as predicted by the hybrid solution in agreement with the experimental data.

If we compare the hybrid method to the full DSMC simulations by Selezneva *et al.* [17], we can notice that the results of the full DSMC simulations and the hybrid method are almost equivalent in the shock and aftershock regions. However, in the near-inlet and expansion regions, especially at 100 Pa chamber pressure, the hybrid approach matches the experimental data better than the full DSMC approach.

We can notice that even if at 20 Pa chamber pressure, the temperature profiles predicted by the DSMC alone and by the hybrid approach are very similar and they both accurately match the experimental data [Fig. 8(a)], increasing the chamber pressure to 100 Pa, and therefore enlarging the continuum region, the differences between the DSMC and the hybrid approach in the near-inlet and expansion regions become more significant [Fig. 8(b)]. The DSMC alone cannot follow the experimental data in the near-inlet and expansion regions, and cannot predict the temperature peak after the shock, while the hybrid solution results are in very good agreement with experiments.

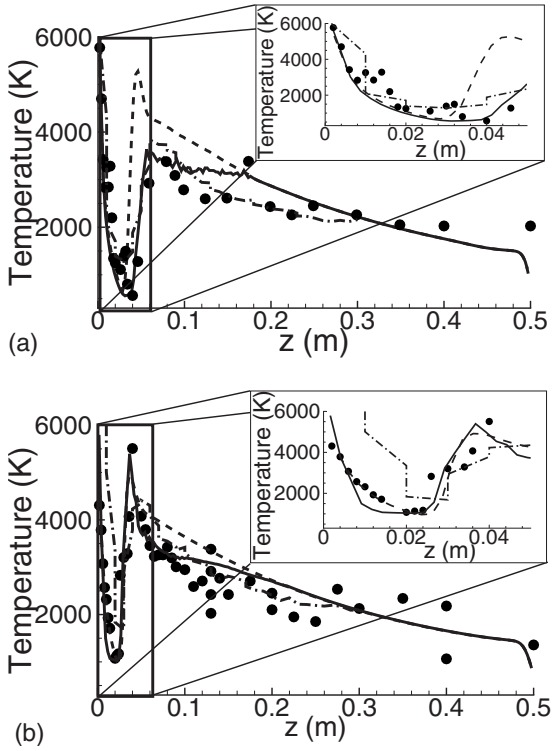

FIG. 8. Temperature distribution along the z axis for 20 Pa (a), and 100 Pa (b) chamber pressures. Continuum (– –), DSMC data from [17] (–·–), hybrid (—), and experimental data from [8] (●).

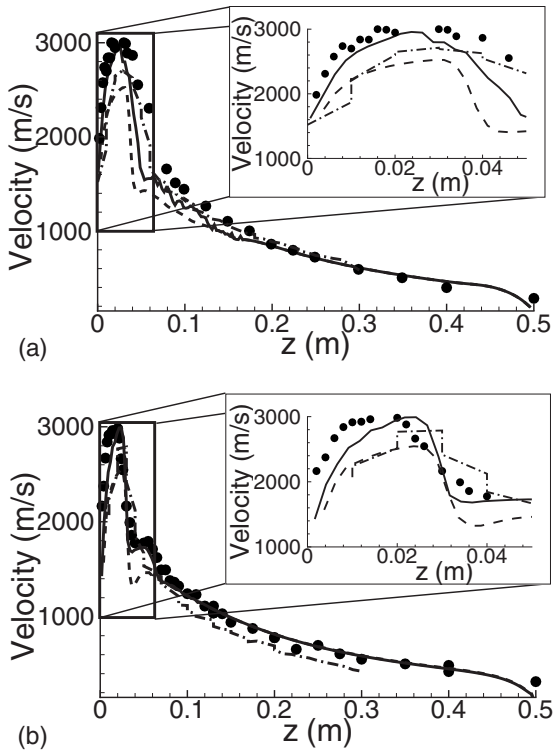

FIG. 9. Velocity profile along the z axis for 20 Pa (a), and 100 Pa (b) chamber pressures. Continuum (– –), DSMC data from [17] (–·–), hybrid (—), and experimental data from [8] (●).

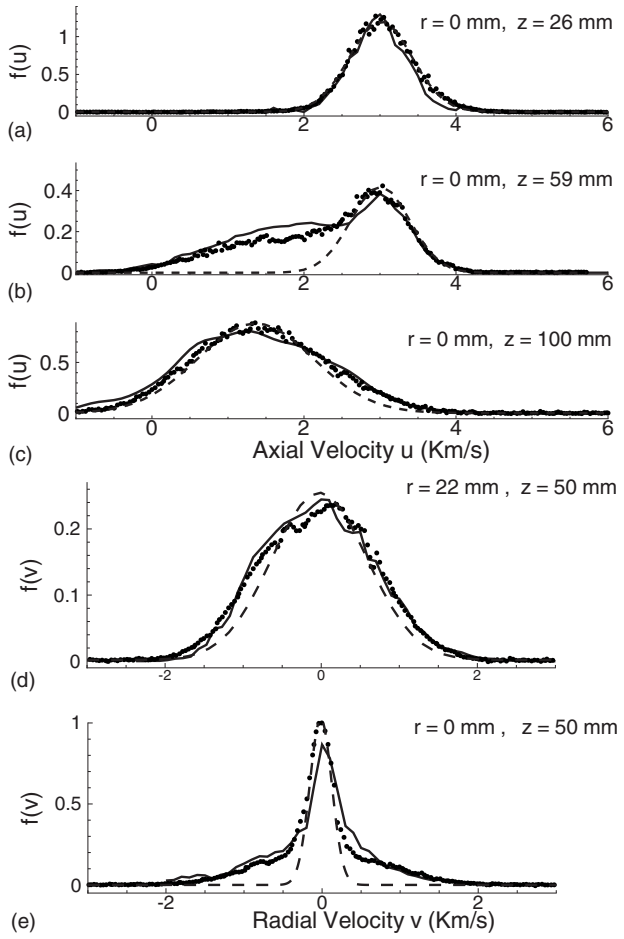

FIG. 10. Axial velocity distribution at $r=0$ and $z=26$ mm (a), $z=59$ mm (b), and $z=100$ mm (c) and radial velocity distribution at axial position $z=50$ mm and radial position $r=0$ (d) and $r=22$ mm (e), for 20 Pa chamber pressure. Hybrid simulation results (—), Maxwellian distribution (– –), and experimental data from [8] (●).

In an analogous manner, from Fig. 9 we can conclude that, because it was not possible to respect DSMC requirements in the near-inlet region, the DSMC method predicts a wrong velocity in this region that influences its solution also in the expansion region. As a result, DSMC predicted a too low value of the maximum velocity reached in the expansion at both 20 Pa and 100 Pa chamber pressures, whereas the hybrid approach accurately predicts these maxima.

B. Invasion of the supersonic region by background particles

In order to study the possible invasion of the supersonic region by the background molecules, during the simulations at 20 Pa chamber pressure, the velocity distribution profiles were recorded at the positions where they have been measured experimentally by Engeln *et al.* [8].

In Figs. 10(a)–10(c), we compare the axial velocity distribution of our simulation at $r=0$, and $z=26$ mm, $z=59$ mm, and $z=100$ mm with the ones measured by Engeln *et al.* In the same way, in Figs. 10(d) and 10(e) we compare Engeln's radial velocity components with our simulated ones at $z=50$ mm and $r=0$ and $r=22$ mm.

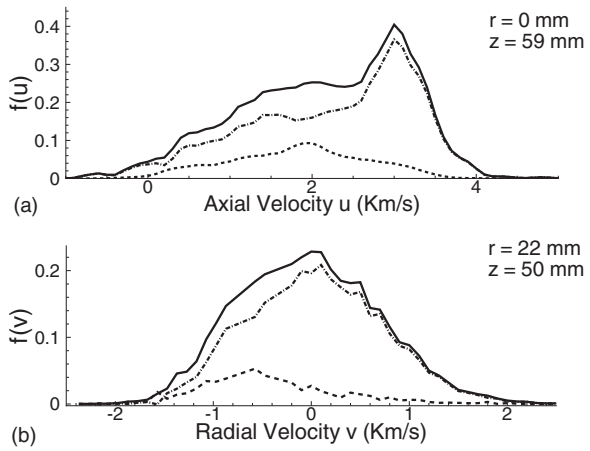

FIG. 11. Relative contribution of background particles to the axial velocity distribution at $r=0$ and $z=59$ mm (a) and to the radial velocity distribution at $r=22$ mm and $z=50$ mm (b), for 20 Pa chamber pressure. Total velocity distribution (—), inlet particles (–·–), and background particles (– –).

In [8], Engeln *et al.* expressed the measured velocity distributions in terms of the intensity of the recorded signal during the experiments and, therefore, the surface area below the experimental data is not equal to 1. In order to be able to compare our numerical data with the measured distributions, in Fig. 10 our curves were scaled by a factor equal to the surface area under the experimental curves. From Fig. 10, it is clear that there is very good agreement between our current hybrid simulations and the experiments from [8].

If we compare the axial and radial velocity distributions of our simulations with a Maxwellian distribution (Fig. 10), we can affirm that downstream of $z \approx 30$ mm there is a clear departure from equilibrium.

In this section we want to demonstrate that this nonequilibrium is due to the invasion of background particles into the expansion-shock region. In continuum conditions, because of the presence of the shock, these particles would not be able to enter the supersonic region. However, we will show that, because of the rarefaction effects, the shock becomes transparent and does not protect the supersonic region. Therefore some particles may actually move into it from the subsonic part of the flow. To demonstrate this hypothesis, it is necessary to know the origin of the particles present in the supersonic region. For this reason, for the particles in the DSMC region, two different labels were used; one for the particles which, after entering the reactor chamber, have always been in the supersonic region (the so-called "inlet particles"), and a different one for the background particles.

In Fig. 11(a) we show the contribution of the background particles and the inlet particles to the axial velocity distribution, at the position $r=0$ and $z=59$ mm, where the departure from the equilibrium is most clear. The presence of background particles in the supersonic region is evident. Once the background particles have penetrated the supersonic region, they start colliding and interacting with the particles that are already there, decelerating them and being accelerated by them. As a result, the velocity distribution of the inlet particles becomes non-Maxwellian.

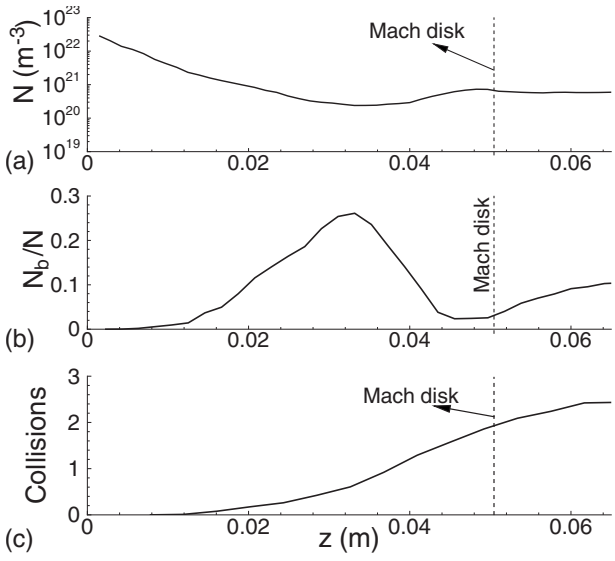

FIG. 12. Number density N (m^{-3}) (a), background particles concentration N_b/N (b), and the number of inlet-background particles collisions (c) along the z axis for 20 Pa chamber pressure.

In an analogous manner, in Fig. 11(b) the contribution of background and inlet particles to the radial velocity distribution at the position $r=22$ mm and $z=50$ mm is shown. It is interesting to note that the peaks of the two contributions are located on opposite sides of the zero velocity position. This means that while particles coming from the inlet are moving away from the axis because of the expansion, the background particles are penetrating into the supersonic region and moving toward the axis.

Experimental indications for the presence of background particles in the expansion-shock region were also found by Engeln *et al.* in [8]. Therefore, our study gives numerical support to the hypothesis of Engeln *et al.* that background particles can penetrate the supersonic region, and, by interacting with the inlet particles can influence the flow field.

In order to further prove the hypothesis of the presence of background particles in the supersonic region and explain how they cause thermodynamic nonequilibrium by colliding and interacting with the local particles, a study was performed in the supersonic region by tracking particles and collisions. The results of this study are presented in Fig. 12.

In Fig. 12(a) we show the number density profile along the z axis in order to clearly locate the expansion region and the shock (Mach disk). The background particles concentration in Fig. 12(b) definitely confirms the presence of invading background particles in the supersonic region. In particular, the figure also shows that they concentrate in the expansion region where the pressure is low. This means that they are driven into the expansion region by favorable pressure gradients, but, for the same reason, once they are there, it is difficult for them to cross the Mach disk because of the adverse pressure gradient.

Finally, Fig. 12(c) presents the average number of collisions with background particles that an inlet particle has undergone before reaching the position along the z axis indicated on the abscissa. As expected, the number of collisions increases along the axis and it reaches the maximum value of 2.4 collisions. This is of course an averaged value, meaning that there are inlet particles which do not collide, as well as inlet particles that have collided much more than 2.4 times with background particles. This clearly demonstrates that the inlet particles do interact with the background particles that invaded the supersonic region.

V. CONCLUSIONS

The gas dynamics of a hot gas jet supersonically expanding into a low pressure (20–100 Pa) chamber is studied by means of a hybrid coupled continuum-DSMC method. This method gives the possibility to save computational time using CFD in most of the domain and to use DSMC only where it is necessary in order to correctly model the flow.

Answers to two main questions about supersonic expansion in a low pressure environment have been found: the importance of taking into account rarefaction effects in modeling the flow and the invasion of the supersonic region by background particles.

We have shown that, because of the presence of rarefaction effects, already at 100 Pa chamber pressure the continuum approach is not suitable to model the flow, while a hybrid continuum-DSMC method can be applied correctly and efficiently. Through an analysis of the velocity distributions and the tracking of particles and collisions in the supersonic region, we have demonstrated the presence of background particles in this region, thus proving the invasion of the supersonic region by background particles passing through the barrel shock.

[1] C. Cai and I. D. Boyd, *36th AIAA Plasmadynamics and Laser Conference AIAA-20054662* (Toronto, Ontario, Canada, 2005).
[2] J. W. A. M. Gielen, W. M. M. Kessels, M. C. M. van de Sanden, and D. C. Schram, J. Appl. Phys. **82**, 2643 (1997).
[3] J. B. Fenn and J. B. Anderson, *Rarefied Gas Dynamics*, edited by J. H. de Leeuw (Academic, New York, 1966), Vol. 2.
[4] R. Campargue, J. Chem. Phys. **52**, 1795 (1970).
[5] M. C. M. Van de Sanden, J. M. de Regt, and D. C. Schram, Plasma Sources Sci. Technol. **3**, 501 (1994).
[6] M. C. M. Van de Sanden, R. van de Bercken, and D. C. Schram, Plasma Sources Sci. Technol. **3**, 511 (1994).
[7] R. F. G. Meulenbroeks, R. A. H. Engeln, M. N. A. Beurskens, R. M. J. Paffen, M. C. M. van de Sanden, J. A. M. van der Mullen, and D. C. Schram, Plasma Sources Sci. Technol. **4**, 74 (1995).
[8] R. Engeln, S. Mazouffre, P. Vankan, D. C. Schram, and N. Sadeghi, Plasma Sources Sci. Technol. **10**, 595 (2001).
[9] S. Mazouffre, M. G. H. Boogaarts, I. S. J. Backer, P. Vankan,

R. Engeln, and D. C. Schram, Phys. Rev. E **64**, 016411 (2001).
[10] S. Mazouffre, M. G. H. Boogaarts, J. A. M. van der Mullen, and D. C. Schram, Phys. Rev. Lett. **84**, 2622 (2000).
[11] J. J. Beulens, G. M. W. Kroesen, P. M. Vallinga, and D. C. Schram, *Proceedings of the International Symposium on Plasma Chemistry ISPC-9* (Pugnochiuso, Italy, 1989).
[12] J. J. Beulens, D. Milojevic, D. C. Schram, and P. M. Vallinga, Phys. Fluids B **3**, 2548 (1991).
[13] K. T. A. L. Burm, W. J. Goedheer, and D. C. Schram, Phys. Plasmas **6**, 2622 (1999).
[14] M. C. M. van de Sanden, J. M. de Regt, and D. C. Schram, Phys. Rev. E **47**, 2792 (1993).
[15] G. M. Janssen, J. van Dijk, D. A. Benoy, M. A. Tas, K. T. A. L. Burm, W. J. Goedheer, J. A. M. van der Mullen, and D. C. Schram, Plasma Sources Sci. Technol. **8**, 1 (1999).
[16] W. M. M. Kessels, A. Leroux, M. G. H. Boogaarts, J. P. M. Hoefnalels, M. C. M. van de Sanden, and D. C. Schram, J. Vac. Sci. Technol. A **19**, 467 (2001).
[17] S. E. Selezneva, M. I. Boulos, M. C. M. de Sanden, R. Engeln, and D. C. Schram, J. Phys. D **35**, 1362 (2002).
[18] P. W. Vankan, *Proceedings of the 24th International Symposium on Rarefied Gas Dynamics* (Monopoli, Italy, 2004).
[19] P. Vankan, D. C. Schram, and R. Engeln, Plasma Sources Sci. Technol. **14**, 744 (2005).
[20] O. Gabriel, P. Colsters, R. Engeln, and D. C. Schram, *Proceedings of the 25th Symposium on Rarefied Gas Dynamics* (St. Petersburg, Russia, 2006).
[21] N. G. Hadjiconstantinou, J. Comput. Phys. **154**, 245 (1999).
[22] P. Le Tallec and F. Mallinger, J. Comput. Phys. **136**, 51 (1997).
[23] H. S. Wijesinghe and N. G. Hadjiconstantinou, Int. J. Multiscale Comp. Eng. **2**, 189 (2004).
[24] A. L. Garcia, J. B. Bell, W. Y. Crutchfield, and B. J. Alder, J. Comput. Phys. **154**, 134 (1999).
[25] J. S. Wu, Y. Y. Lian, G. Cheng, R. P. Koomullil, and K. C. Tseng, J. Comput. Phys. **219**, 579 (2006).
[26] T. E. Schwartzentruber and I. D. Boyd, J. Comput. Phys. **215**, 402 (2006).
[27] G. Abbate, B. J. Thijsse, and C. R. Kleijn, special issue of Int. J. Multiscale Comp. Eng. (to be published).
[28] S. E. Selezneva, M. Rajabian, D. Gravelle, and M. I. Boulos, J. Phys. D **34**, 2862 (2001).
[29] M. C. M. van de Sanden, J. M. de Regt, G. M. Jansen, J. A. M. van der Mullen, D. C. Schram, and B. van der Sijde, Rev. Sci. Instrum. **63**, 3369 (1992).
[30] S. Y. Chou and D. Baganoff, J. Comput. Phys. **130**, 217 (1997).
[31] T. Lou, D. C. Dahlby, and D. Baganoff, J. Comput. Phys. **145**, 489 (1998).
[32] J. O. Hirschfelder, C. F. Curtis, and R. B. Bird, *Molecular Theory of Gases and Liquids*, 4th ed. (Wiley, New York, 1954).
[33] G. A. Bird, *Molecular Gases Dynamics and the Direct Simulation of Gas Flows* (Clarendon Press, Oxford, 1998).
[34] R. P. Nance, D. B. Hash, and H. A. Hassan, J. Thermophys. Heat Transfer **12**, 447 (1998).
[35] A. L. Garcia and B. J. Alder, J. Comput. Phys. **140**, 66 (1998).
[36] A. L. Garcia, J. B. Bell, W. Y. Crutchfield, and B. J. Alder, J. Comput. Phys. **154**, 134 (1999).
[37] D. Hash and H. Hassan, AIAA Pap. 96–0353 (1996).
[38] W.-L. Wang and I. D. Boyd, *40th AIAA Aerospace Sciences Meeting and Exhibit*, Reno, NV (2002).